# New measurement of the refractive, elastic $^{16}$O+$^{12}$C scattering at 132, 170, 200, 230, and 260 MeV incident energies

A. A. Ogloblin,[1] Yu. A. Glukhov,[1,2] W. H. Trzaska,[2] A. S. Dem'yanova,[1,2] S. A. Goncharov,[3] R. Julin,[2] S. V. Klebnikov,[2,4] M. Mutterer,[5] M. V. Rozhkov,[1,2] V. P. Rudakov,[1] G. P. Tiorin,[2,4] Dao T. Khoa,[6] and G. R. Satchler[7]

[1]*RSC ''Kurchatov Institute,'' RU-123182 Moscow, Russia*
[2]*Department of Physics, Jyväskylä University, FIN-40351 Jyväskylä, Finland*
[3]*Institute of Nuclear Physics, Moscow State University, RU-119899 Moscow, Russia*
[4]*V. G. Khlopin Radium Institute, RU-197022 St. Petersburg, Russia*
[5]*Technical University Darmstadt, Schlossgartenstrasse 9, D-64289 Darmstadt, Germany*
[6]*Institute for Nuclear Science & Technique, VAEC, P.O. Box 5T-160, Nghia Do, Hanoi, Vietnam*
[7]*Physics Division, Oak Ridge National Laboratory, Oak Ridge, Tennessee 37831-6373*
*and Department of Physics & Astronomy, University of Tennessee, Knoxville, Tennessee 37996-1200*

For the first time, differential cross section of the $^{16}$O+$^{12}$C elastic scattering at $E_{lab}$=170, 200, 230, and 260 MeV has been measured over a wide angular range which covers both diffractive and refractive regions. In addition, the recent data at 132 MeV for this system have been remeasured with much better statistics. A well developed rainbow structure has been observed, where up to three Airy minima could be identified in each measured angular distribution. The optical model analysis of these data was done using the conventional Woods-Saxon shape for the optical potential as well as that given by the folding model. The Airy systematics enabled us to suggest a realistic family of the optical potential for the $^{16}$O+$^{12}$C system, which consistently describes the new data as well as the data measured earlier at incident energies of 608 and 1503 MeV. Our results show that the $^{16}$O+$^{12}$C system is a very suitable heavy-ion combination for the study of refractive phenomena, which can give important information on the nucleus-nucleus potential at small distances.

PACS number(s): 25.70.Bc, 24.10.Ht, 21.30.Fe

## I. INTRODUCTION

The past decade has seen significant progress in our understanding of the heavy-ion (HI) optical potential that describes the elastic scattering of two nuclei [1], especially through studies of elastic scattering of certain combinations of light heavy-ions, for which the absorption is relatively weak and refractive effects appear. Refractive (rainbow) phenomena in nuclear scattering provide a unique source of information on the HI interaction potential at small internuclear distances [1,2]. So far, systematic experimental evidence of nuclear rainbow in light HI scattering has been found mainly in two symmetric systems: $^{12}$C+$^{12}$C and $^{16}$O+$^{16}$O; with the most spectacular Airy pattern exhibited in elastic $^{16}$O+$^{16}$O scattering at $E_{lab}$=350 MeV [3]. When refractive effects, in particular, nuclear rainbows are discernible, very important information about the shape and strength of the real optical potential can be obtained. For example, high-precision refractive scattering data have been used in the folding analyses [4,5] to probe the density dependence of the effective in-medium nucleon-nucleon ($NN$) interaction and to place constraints upon the value of the incompressibility of cold nuclear matter (a key quantity in specifying the nuclear equation of state).

While the $^{12}$C+$^{12}$C and $^{16}$O+$^{16}$O systems are quite ''transparent'' for refractive effects to appear, the Mott interference caused by the boson symmetry between the two identical nuclei sometimes leads to rapidly oscillating elastic cross sections at angles around $\theta_{c.m.}$=90°, which in turn obscure Airy structures in this angular region. The whole Airy

pattern might only be seen in an optical model (OM) calculation which removes the symmetrization artificially [6,7]. Therefore, the study of a nonidentical *refractive* light HI system should be an interesting alternative, which could reveal the Airy pattern of rainbow supernumeraries [2] over the whole angular range. The $^{16}$O+$^{12}$C system does not have the boson symmetry, and was suggested as a good candidate for the study of nuclear rainbow [8]. However, the available elastic data for this system (at $E_{lab}$=24, 35, and 42 MeV [9]; 65 and 80 MeV [10]; 139, 215, and 311 MeV [11]) cover only limited angular intervals and do not allow to reveal any feature of the refractive scattering. At higher energies, there are two data sets available for the $^{16}$O+$^{12}$C system which have been measured at $E_{lab}$=608 MeV [12] and 1503 MeV [13]; but the data at the former energy do not extend to sufficiently large angles to identify the Airy pattern [14], while the latter energy is too high to observe the ''rainbow'' unambiguously, since the refractive part of the angular distribution has moved forward and mixed with the diffractive part at forward angles.

The elastic $^{16}$O+$^{12}$C data at $E_{lab}$=132 MeV [15], which were measured first in our extensive experimental study of the $^{16}$O+$^{12}$C elastic scattering, have clearly shown a pronounced rainbow pattern associated with the second order Airy minimum. This result has encouraged us to carry on experiment on the elastic $^{16}$O+$^{12}$C scattering at other energies. The present article reports on our new measurement of the elastic $^{16}$O+$^{12}$C scattering at $E_{lab}$=170, 200, 230, and 260 MeV, which was aimed to study the evolution of the refractive (Airy) pattern in the $^{16}$O+$^{12}$C system in this en-

ergy range. To extract a reliable energy dependence of the $^{16}O+{}^{12}C$ optical potential, the elastic data at 132 MeV for this system [15] have been remeasured with a much better statistics, at angles up to $\theta_{c.m.} \approx 173°$. The new data have been analyzed within the optical model (OM) using the conventional Woods-Saxon shape for the optical potential as well as that given by the double-folding model [5]. The systematics for the evolution of the Airy structure in the $^{16}O+{}^{12}C$ system is given and a realistic family of the optical potential for this system is suggested, which consistently describes the new data as well as the data measured earlier at incident energies of 608 [12] and 1503 MeV [13].

## II. EXPERIMENT

The $^{16}O+{}^{12}C$ scattering experiment was carried out at Jyväskylä University Cyclotron, which provided the oxygen $5^+$ or $6^+$ beam of the required energy with an intensity of about 100 nA (electrical). The energy resolution of the beam was around 0.3%, the diameter of the beam spot about $2 \times 3$ mm$^2$. A scattering chamber of the diameter $\approx 1500$ mm was used for the measurements. The targets were self-supporting carbon foils of 0.24 mg/cm$^2$ thickness. The detectors were located on two turn-around tables and could be rotated in the full angular range. Three types of detector systems were used for the measurements in different angular ranges.

(i) The cross sections at forward angles ($\theta_{c.m.} = 7° - 40°$) were measured by a $\Delta E - E$ telescope consisting of semiconductor counters. The thickness of $E$ and $\Delta E$ counters was 600 and 25 $\mu$m, respectively. The solid angle covered by the telescope was about 0.08 msr. The total energy resolution (determined by the kinematics) was 1.2 MeV. The angular resolution was $\pm 0.2°$ and was determined mainly by the beam angular spread.

(ii) For the measurements in the medium angular range ($\theta_{c.m.} = 40° - 80°$) a position-sensitive $\Delta E - E$ detector was used. It included a gas-filled proportional $\Delta E$ counter with variable pressure, and a $E$ detector consisting of ten silicon pin-diodes of $10 \times 10$ mm dimension each and thickness of 380–760 $\mu$m. This detector can cover the angular range of about 10° in the laboratory system.

(iii) The scattering events at larger angles ($\theta_{c.m.} = 80° - 130°$) were measured using kinematical coincidences. Two silicon detectors of the sizes $30 \times 30$ mm and $100 \times 10$ mm (in the latter case the position-sensitive detector mentioned above was used without its $\Delta E$ part) were located on the both sides of the beam, at the distances of 600 mm and 300 mm from the target, respectively. The identification of the elastic scattering events was done by measuring the total deposited energy. The necessary corrections for the geometry were made properly. Selected events were recorded event-by-event and treated offline. The accuracy of the absolute cross-section measurement was estimated to be around 15%.

## III. RESULTS AND DISCUSSIONS

The measured elastic data (in ratio to Rutherford cross section) are plotted in Figs. 1 and 2. To show the evolution

of the refractive pattern in the elastic $^{16}O+{}^{12}C$ scattering, the data measured earlier at $E_{lab} = 608$ MeV [12] are also presented. We note that the data at 132 MeV have been remeasured by the Kurchatov group with a much better statistics. In comparison with the original data published in Ref. [15], the new data set contains much more points at angles $\theta_{c.m.} > 100°$. The enhancement in the backward cross section measured at 132 MeV is expected to be due to other processes, like the elastic ($Q=0$) alpha transfer process $^{12}C(^{16}O,{}^{12}C)^{16}O$ [16]. We note that preliminary results of the CRC calculation [17] for elastic alpha transfer in the $^{16}O+{}^{12}C$ system at 132 MeV obtained with the WS1 optical potential (Table I) show that the elastic alpha transfer can indeed enhance elastic cross sections at large angles, although the effect still depends strongly on the parameters used to calculate the wave function of the alpha particle bound in $^{16}O$ nucleus, and the spectroscopic factors assumed. This aspect needs a separate and more extensive study, including measurements on the $^{12}C$ produced at forward angles. As for the results of the OM analysis, we will see below that all conclusions drawn in Ref. [15] for this energy remain practically the same.

In the OM analysis of the present data, we have used the conventional six-parameter Woods-Saxon (WS) form for the complex optical potential

$$U(R) = V_C(R) - V\left[1 + \exp\left(\frac{R-R_V}{a_V}\right)\right]^{-1}$$
$$- iW\left[1 + \exp\left(\frac{R-R_W}{a_W}\right)\right]^{-1}, \qquad (1)$$

where

$$R_{V,W} = r_{V,W}(16^{1/3} + 12^{1/3}).$$

The WS parameters were adjusted to obtain the least $\chi^2$ fit to the scattering data. To increase the weight of the data points at large angles which are especially sensitive to the strength and shape of the optical potential at small distances, we have assumed a 10% uncertainty for all data points. The potential parameters obtained from the OM fit to the data at 132, 170, 200, 230, and 260 MeV are listed in Table I.

A folding model analysis has also been performed. In this case, the real optical potential, $V_F(R)$, is calculated within a generalized version of the double-folding model [5,18], using the newly parametrized (CDM3Y6) density-dependent M3Y interaction based on the $G$-matrix elements of the Paris $NN$ potential (see details in Ref. [5]). The nuclear densities used in the folding model calculations were taken as Fermi distributions with parameters [19] chosen to reproduce the shell-model densities for $^{16}O$ and $^{12}C$ and which give the rms charge radii deduced from electron scattering. The optical potential in such a folding analysis is

$$U(R) = V_C(R) + N_R V_F(R) - iW\left[1 + \exp\left(\frac{R-R_W}{a_W}\right)\right]^{-1}, \qquad (2)$$
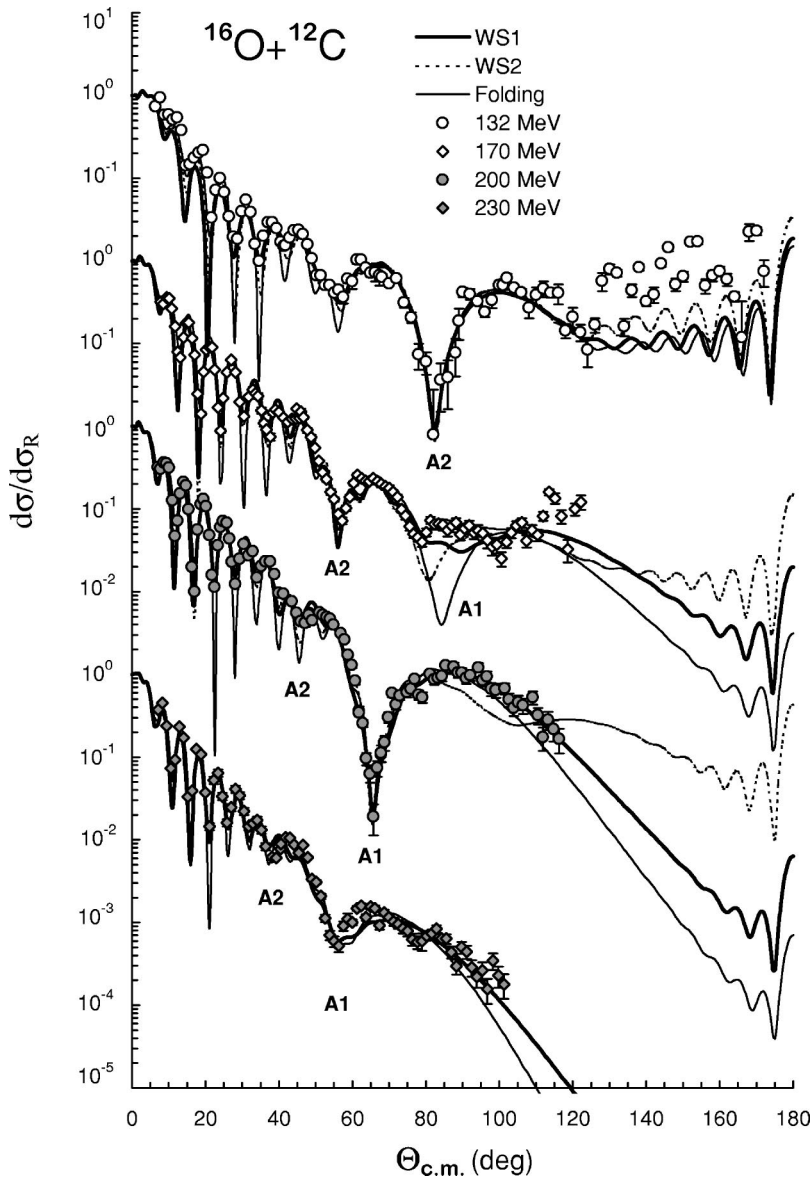
FIG. 1. Measured elastic $^{16}$O + $^{12}$C scattering data at $E_{lab}$ = 132, 170, 200, and 230 MeV in comparison with the OM fits given by the folding potential and by two different families (WS1 and WS2) of the optical potential of Woods-Saxon shape (see Table I). A $k$ indicates the $k$th order Airy minimum in the far-side cross section given by the folding or WS1 set of the optical potential.

where the renormalization factor $N_R$ together with the parameters of the imaginary potential were adjusted to fit the data. We note that the main features of the new version of the folding model [5,18] are the inclusion of a realistic density dependence into the effective *NN* interaction and the explicit treatment of the exchange potential using a realistic local approximation for the nonlocal (one-body) density matrix. The localizing procedure for the nuclear one-body density matrix requires the evaluation of the kinetic energy density $\tau$. In our previous folding calculations [4,5,20], the so-called Weizsäcker strength of the surface contribution to $\tau$ was usually taken to equal 1/4. However, recent studies [21] of the one-particle exchange in the folding model have shown that the more correct value of Weizsäcker term is 1/36. Such a value is now used in the calculation of the folding potential, and this results in a slightly smaller renormalization factor $N_R$ of the best-fit folding potential (Table I) compared to that obtained in our previous folding analyses for this system [5,15].

The Coulomb potential $V_C(R)$, used in the folding calculation and in the OM analysis, was generated by folding two uniform charge distributions of radii $R_C$ = 3.54 and 3.17 fm, for $^{16}$O and $^{12}$C, respectively, which have rms charge radii close to those extracted from the electron scattering data. All the OM analyses were made using the code PTOLEMY [22]. We note that the inputs for masses and c.m. energies in the folding calculation of $V_F(R)$ as well as in the OM analysis were taken as given by the relativistically corrected kinematics [23].

For the data at 132 and 170 MeV, our six-parameter OM search resulted in several local $\chi^2$ minima; corresponding to these, two families of discrete WS sets (WS1 and WS2) are listed in Table I. While the imaginary WS potentials are more or less of the same strength, the obtained real WS potentials have different depths which result in different volume integrals per interacting nucleon pair $J_V$. In the tail region they all have about the same strength to reproduce the Fraunhofer diffraction correctly. The folding model analysis gives results quite close to those given by the WS1 family of the WS optical potential. The best-fit WS parameters for the
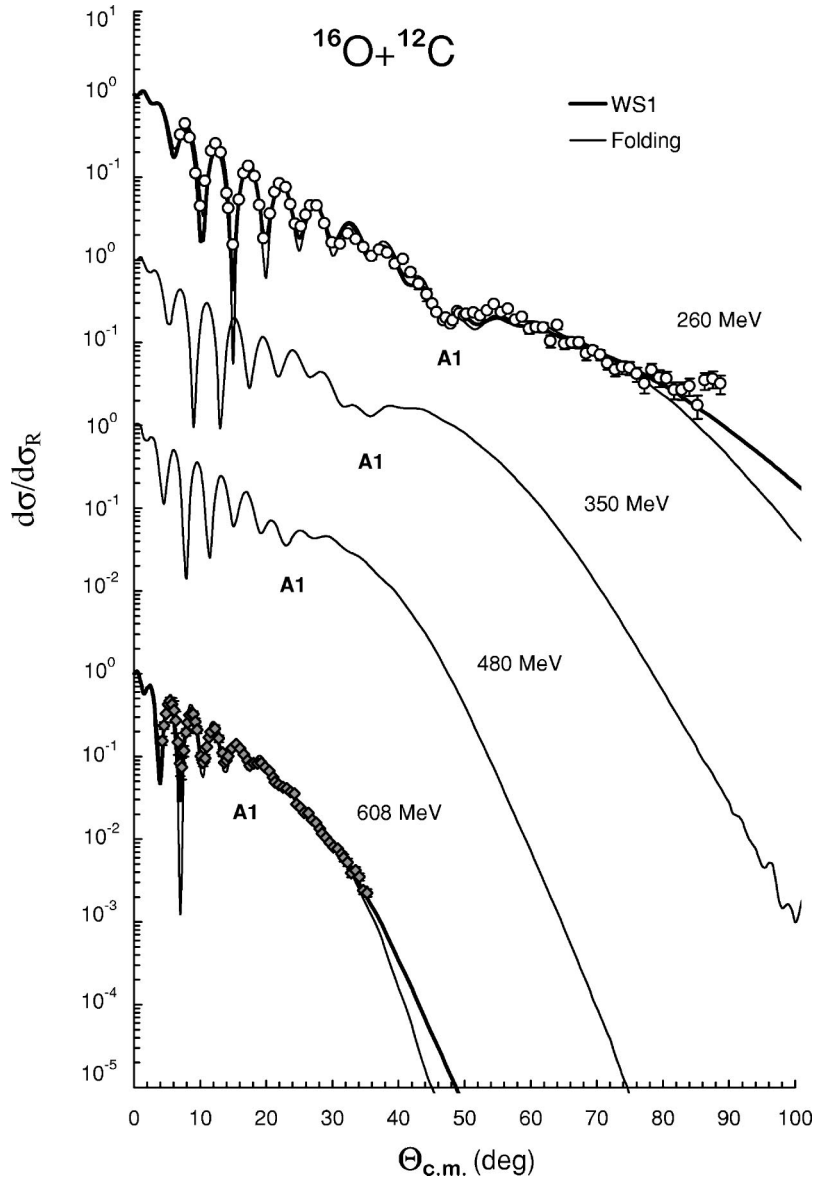
FIG. 2. Measured elastic $^{16}O + ^{12}C$ scattering data at $E_{lab} = 260$ and $608$ MeV in comparison with the OM fits given by the folding potential and by the WS1 set of the optical potential (see Table I). The folding prediction for elastic $^{16}O + ^{12}C$ scattering at $E_{lab} = 350$ and $480$ MeV was done using the OM parameters interpolated from those at neighboring energies. A1 indicates the first order Airy minimum in the far-side cross section given by the folding or WS1 set of the optical potential.

imaginary potential as well as the volume integrals of the real ($J_V$) and the imaginary ($J_W$) potentials given by the best-fit WS1 and folding potentials show that these potentials belong practically to the same potential family (for the real $^{16}O + ^{12}C$ optical at the considered energies). From the descriptions of the elastic data given by the WS1 set of WS potential and by the folding potential shown in Figs. 1 and 2, one can see that they all provide reasonable fits to the data. The refractive structure of the cross section at large angles given by the WS1 potential and by the folding potential has the same refractive origin.

Based on the study of the evolution of the refractive pattern in the elastic $^{16}O + ^{12}C$ scattering in our previous work [15], it can be shown that the observed minimum at $\theta_{c.m.} \approx 82°$ in the measured angular distribution at 132 MeV is described as the second (A2) or third (A3) order Airy minimum by the WS1 or WS2 sets of the optical potential (see Table I), respectively. The best-fit folding potential is quite close in shape to the WS1 potential and also describes this minimum as A2.

At 170 MeV the second Airy minimum is shifted to a smaller angle ($\theta_{c.m.} \approx 57°$) while some oscillation structure is seen at angles $\theta_{c.m.} \approx 80° - 120°$. However, the modulation pattern at large angles is more complicated than that expected from the A1 minimum which is always followed by a broad primary rainbow maximum (see, e.g., prediction given by the folding potential shown in Fig. 1). A more flexible WS shape of the real optical potential also cannot be fitted to reproduce the oscillating structure at largest angles in the 170 MeV data. This might indicate that other nonscattering events, like the elastic alpha transfer process mentioned above, still contribute to the elastic cross section at energy of 170 MeV.

At higher energies, especially, for the incident energies of 200, 230, and 260 MeV, one can clearly observe broad oscillation of the Airy structure at large angles. A prominent minimum at $\theta_{c.m.} \approx 66°$, $56°$, and $47°$ seen in the data at 200, 230, and 260 MeV, respectively, is followed by a broad shoulderlike maximum with its exponential falloff tail which is typical for the primary rainbow (observed, e.g., earlier in

TABLE I. Optical potential parameters used in the OM analysis of the elastic $^{16}O + ^{12}C$ data at $E_{lab} = 132$–$1503$ MeV. $\chi^2$ values are per datum, and were obtained with uniform 10% errors. Folding parameters at $E_{lab} = 350$ and 480 MeV are interpolated from those at neighboring energies.

| $E_{lab}$ (MeV) | Potential | $V$ (MeV) | $r_V$ (fm) | $a_V$ (fm) | $J_V$ (MeV fm³) | $W$ (MeV) | $r_W$ (fm) | $a_W$ (fm) | $J_W$ (MeV fm³) | $\sigma_R$ (mb) | $\chi^2$ |
|---|---|---|---|---|---|---|---|---|---|---|---|
| 132 | Folding | 0.798 [a] | | | 307.1 | 13.41 | 1.224 | 0.627 | 66.19 | 1507 | 25.9 |
| | WS1 | 282.2 | 0.586 | 0.978 | 304.0 | 13.86 | 1.183 | 0.656 | 62.99 | 1505 | 23.4 |
| | WS2 | 361.8 | 0.653 | 0.807 | 404.3 | 16.38 | 1.152 | 0.662 | 69.39 | 1483 | 21.1 |
| 170 | Folding | 0.787 [a] | | | 296.6 | 17.46 | 1.227 | 0.582 | 85.76 | 1530 | 19.0 |
| | WS1 | 255.5 | 0.629 | 0.967 | 310.9 | 16.27 | 1.245 | 0.514 | 81.73 | 1494 | 10.2 |
| | WS2 | 333.4 | 0.604 | 0.920 | 355.9 | 17.94 | 1.231 | 0.526 | 87.58 | 1500 | 14.1 |
| 200 | Folding | 0.771 [a] | | | 285.9 | 17.67 | 1.242 | 0.526 | 88.51 | 1494 | 14.2 |
| | WS1 | 216.3 | 0.683 | 0.927 | 299.8 | 17.83 | 1.219 | 0.541 | 84.97 | 1494 | 7.1 |
| | WS2 | 314.7 | 0.625 | 0.908 | 355.8 | 19.18 | 1.224 | 0.524 | 91.98 | 1498 | 10.7 |
| 230 | Folding | 0.774 [a] | | | 282.7 | 21.28 | 1.186 | 0.604 | 95.65 | 1528 | 12.5 |
| | WS1 | 179.9 | 0.763 | 0.836 | 293.0 | 22.30 | 1.162 | 0.638 | 95.78 | 1550 | 9.2 |
| 260 | Folding | 0.772 [a] | | | 277.6 | 22.52 | 1.177 | 0.565 | 97.76 | 1471 | 8.9 |
| | WS1 | 174.3 | 0.769 | 0.831 | 288.7 | 23.45 | 1.163 | 0.578 | 98.91 | 1481 | 5.6 |
| 350 | Folding | 0.770 [a] | | | 264.2 | 22.00 | 1.150 | 0.600 | 90.63 | 1440 | |
| 480 | Folding | 0.770 [a] | | | 247.0 | 22.00 | 1.150 | 0.600 | 90.63 | 1408 | |
| 608 | Folding | 0.750 [a] | | | 225.3 | 23.74 | 1.129 | 0.603 | 93.02 | 1365 | 9.7 [b] |
| | WS1 | 158.2 | 0.703 | 0.931 | 233.1 | 23.97 | 1.106 | 0.646 | 90.08 | 1374 | 2.4 [b] |
| 1503 | Folding | 0.813 [a] | | | 156.3 | 16.74 | 1.159 | 0.771 | 75.15 | 1316 | 11.3 [b] |
| | WS1 | 77.99 | 0.886 | 0.767 | 173.8 | 24.18 | 1.041 | 0.818 | 83.55 | 1289 | 2.0 [b] |

[a]Renormalization coefficient $N_R$ for the folding potential.
[b]$\chi^2$ values obtained with the experimental errors.

the elastic $^{16}O + ^{16}O$ scattering at $E_{lab} = 350$ MeV [3]). The OM fit shows consistently that the WS1 potential is the most appropriate and it reproduces this minimum in the data at 200, 230, and 260 MeV as the first Airy minimum (A1). The best-fit folding potential belongs practically to the same family as the WS1 potential and also describes these minima as A1. A deeper WS potential belonging to the WS2 family could only be found at $E_{lab} = 132$, 170, and 200 MeV and it gives much worse fit to the data at 200 MeV (see Fig. 1) and clearly fails to reproduce the broad rainbow maximum observed at $\theta_{c.m.} \approx 80° - 120°$.

Although there are no elastic $^{16}O + ^{12}C$ data available at the incident energy around 350–500 MeV, the evolution of the rainbow pattern associated with the first Airy minimum can be qualitatively studied using the prediction of the folding model. As will be discussed below, the energy dependence of the microscopic folded potential has been proven to be quite accurate, and the best-fit folding potentials for the $^{16}O + ^{12}C$ system at the considered energies were found to have a renormalization coefficient $N_R \approx 0.77 \pm 0.04$ (see Table I). Consequently, the folding potential, calculated for the $^{16}O + ^{12}C$ system at an incident energy up to about 1 GeV and renormalized by a factor $N_R = 0.77$, should be a reliable choice of the real optical potential for the $^{16}O + ^{12}C$ system. We have chosen for this study the incident energies of 350 and 480 MeV. The extensive $^{16}O + ^{16}O$ elastic data at these two energies have been shown to have a strong rainbow structure, especially, the 350 MeV data [3,25], and it is natural to expect strong refractive effects in the $^{16}O + ^{12}C$ system

at these energies. The results given by the (real) folding potential calculated at these energies and renormalized by $N_R = 0.77$ are shown in Fig. 2. The WS form was used for the imaginary part of the optical potential, and its parameters were interpolated from the best-fit (imaginary) WS parameters at neighboring energies. One can see from Fig. 2 that the shoulderlike primary rainbow can still be seen at these two energies, and a further measurement of elastic $^{16}O + ^{12}C$ scattering at these energies would be essential for a complete study of the refractive structure in the elastic $^{16}O + ^{12}C$ scattering, in particular, the evolution of the first Airy minimum from $\theta_{c.m.} \approx 47°$ at 260 MeV to $\theta_{c.m.} \approx 15°$ at 608 MeV. We note that the WS1 potential obtained for the 608 MeV data is practically the same WS potential (also dubbed as WS1) proposed in Ref. [14]. As one can see from Fig. 2, the observed exponential falloff of the cross section is well reproduced by both the WS1 and the folding potentials, and it is the remnant of primary rainbow maximum which is somewhat obscured by the diffraction. This result shows that an incident energy $E_{lab} \gtrsim 600$ MeV is already too high for the observation of the (primary) rainbow structure in the $^{16}O + ^{12}C$ system, because the refractive part of the angular distribution is shifted to such small angles that it becomes mixed with the diffractive part.

More insight into the diffractive and refractive phenomena can be provided by the representation of the elastic scattering amplitude in terms of the near-side and far-side components [24]. In this representation, the Fraunhofer diffraction pattern in the elastic scattering cross section at
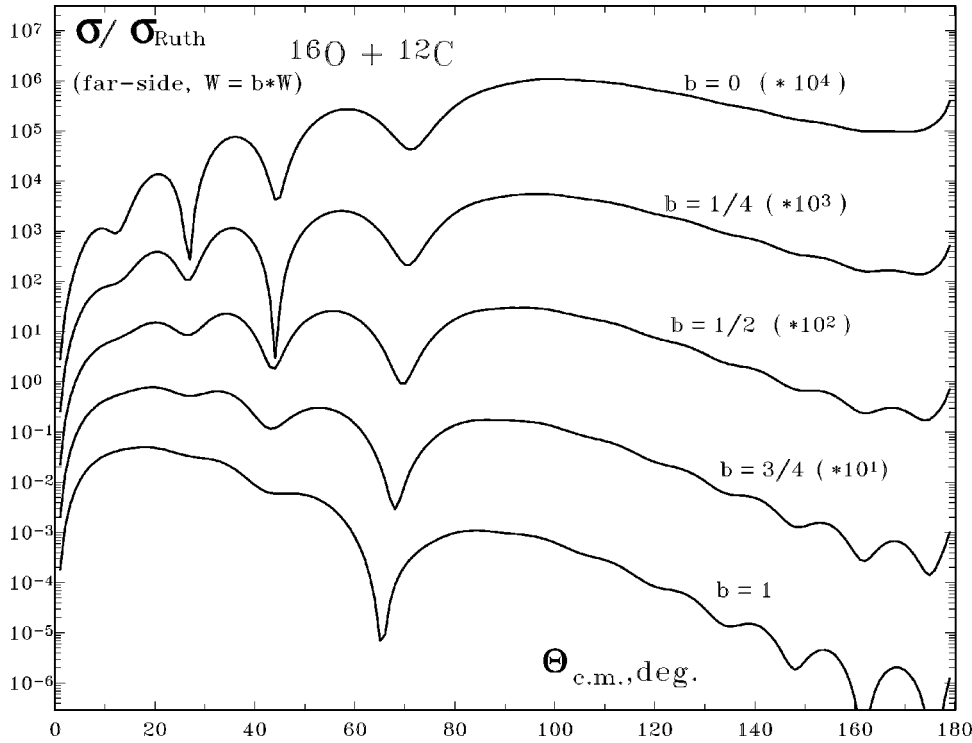
FIG. 3. The far-side cross sections for the $^{16}O + {}^{12}C$ elastic scattering at $E_{lab} = 200$ MeV calculated with different absorption strengths. $b$ is the ratio of the chosen $W$ value to that given by the WS1 set of the complex optical potential which best fits the data.

small angles is due to an interference between the near- and far-side amplitudes in forward direction. At large angles, the elastic scattering pattern of a light heavy-ion system (like $^{16}O + {}^{12}C$ or $^{16}O + {}^{16}O$) is usually determined by the ''refraction'' of the far-side trajectories, when the absorption is not too strong. In such a case, if one can measure the experimental cross section down to $d\sigma/d\sigma_R \approx 10^{-5}$, very valuable information on the real optical potential can be obtained.

The Airy oscillation discussed above is built up by an interference between the $l_<$ and $l_>$ components of the (real) far-side amplitude, which correspond to trajectories coming at the scattering angle $\theta$ with angular momenta $l < l_R$ and $l > l_R$, where $l_R$ is the rainbow angular momentum associated with the minimum of the deflection function $\theta(l)$ (see also discussions in Refs. [1,2,26,27]). Since the $l_<$ subamplitude is usually suppressed by absorption, the Airy oscillating pattern in turn is also obscured by the absorptive imaginary potential. In order to illustrate the Airy pattern of the new data, we have performed the near-far decomposition of the elastic scattering amplitude given by the WS1 set of the optical potential, with the *reduced* strength of the imaginary part. The calculated far-side cross sections for the incident energy of 200 MeV are plotted in Fig. 3, where the Airy minima from the first to the third order are all visible in the angular region if the absorption strength is reduced to zero. With the increasing absorption, the second and third Airy minima become gradually suppressed but the first Airy minimum (followed by a broad primary rainbow maximum) is still to be seen, and it has been clearly observed in the measurement. Our results plotted in Fig. 3 have confirmed again that the location of the Airy minima in the elastic angular distribution remains practically the same if different imaginary potentials are used with the same real optical potential. In other word, the Airy pattern at large angles is mainly

determined by the *real* optical potential used in the OM calculation. Therefore, the new data are very important in specifying the most realistic family of the real optical potential.

It should be emphasized that an interference of $l_<$ and $l_>$ components with comparable strengths would result in a deep Airy minimum if there were no absorption in the system. The absorption damps the $l_<$ components of the amplitudes with small $l$ which correspond to small impact parameters, and hence the deep Airy minima at small angles are smeared out. This effect can be clearly seen in Fig. 3. With the zero absorption, the most prominent Airy minimum is of the third order (A3). When $W$ is set to equal 1/4 of its real strength, the most favorable condition for a strongest interference fulfills for the second Airy minimum (A2) which becomes the deepest. The increase of the absorption strength to 0.5 or 0.75 of the actual value $W$ gradually ''kills'' this minimum but still is not strong enough to rearrange the crossover of $l_<$ and $l_>$ components at the position of the primary rainbow minimum. With the full absorption, the most favorable condition for a strongest interference turns to the first Airy minimum (A1), and this is the situation observed in the experiment. A similar effect was seen also in the 132 MeV data (see Fig. 4 in Ref. [15]), where the half-absorption makes the A3 minimum to be the deepest, while the full absorption makes the most prominent the A2 one.

We have further plotted in Fig. 4 the far-side cross sections obtained for different energies using the WS1 and WS2 sets of the optical potential (Table I) with the zero absorption ($W = 0$). One can clearly see the evolution of the Airy oscillation or supernumerary rainbows with the increasing incident energy. The WS2 set of optical potential gives a reasonable description to the data at the two lowest energies but fails completely to describe the broad (primary) rainbow maximum observed in the 200 MeV data, because it gener-
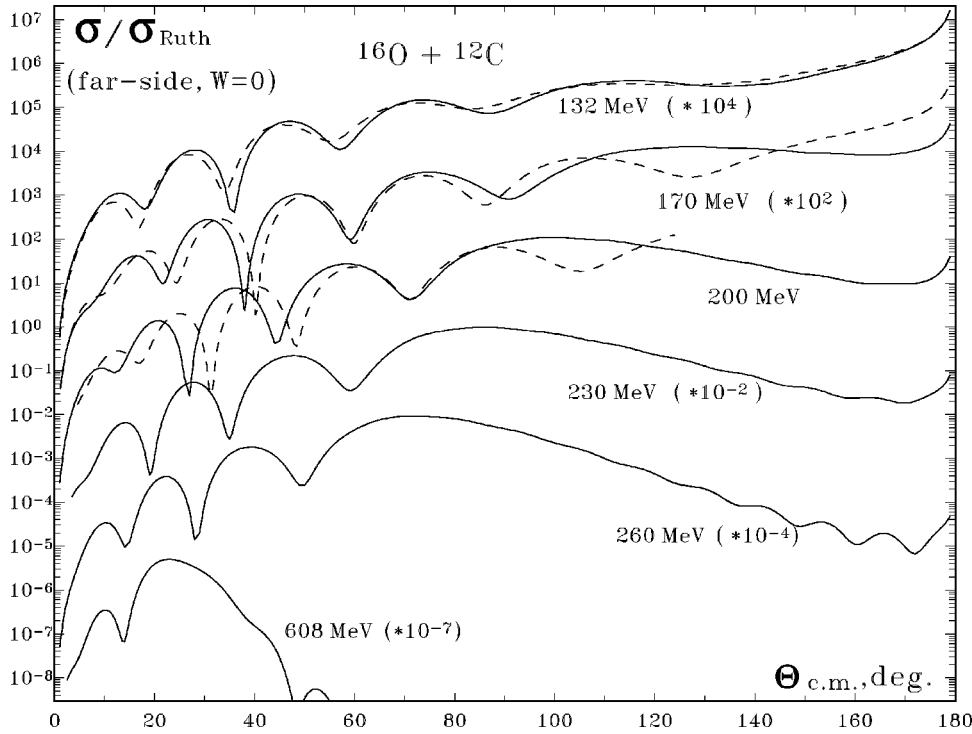
FIG. 4. The far-side cross sections for the $^{16}O + ^{12}C$ elastic scattering at different energies calculated using the WS1 (solid curves) and WS2 (dashed curves) sets of the optical potential (Table I) with the zero absorption ($W=0$).

ates a wrong order for the Airy minima and the primary rainbow (dotted line in Figs. 1 and 4) appears, therefore, at angles much larger than those observed in the data. This fact, together with the Airy systematics discussed below, allows us to suggest that the most realistic is the WS1 (or folding) family of the optical potential which gives an evolution of the refractive Airy structure as shown in Figs. 1 and 2.

It has been suggested by Knoll and Schaeffer [27] that the position of the classical (nuclear) rainbow angle $\theta_{NR}$ shifts with the energy as $1/E$. If one uses the WS shape (1) for the real optical potential, $\theta_{NR}$ can be approximately evaluated as

$$\theta_{NR} \simeq \theta_{CR} - 0.56 \left( \frac{V}{E_{c.m.}} \right) \left( \frac{R_V}{a_V} \right)^{1/2}, \qquad (3)$$

where $\theta_{CR}$ is the Coulomb rainbow angle which is almost constant in the considered cases ($\theta_{CR} \approx 1.5°$ in the c.m. frame). Within this assumption, it is expected that the Airy minima of different orders should lie on different straight (const-$1/E_{c.m.}$) lines. The positions of those minima which can be extracted from the present data and considered as Airy ones are shown in Fig. 5 as the solid circles. As already mentioned, the location of the Airy minima in the elastic angular distribution is determined mainly by the real optical potential, so we have plotted in Fig. 5, as open circles (connected by dashed lines), the minima of the theoretical elastic cross sections shown in Fig. 4 which have been obtained using the WS1 set of the optical potential (Table I) with the zero absorption ($W=0$).

One can see from Fig. 5 that the three most pronounced minima observed in experiment at 200, 230, and 260 MeV and identified in our discussion above as the first Airy minima (followed by the corresponding primary rainbows) are lying practically on the same straight line as expected

from Eq. (3). The A1 minima calculated for the same energies, using the WS1 set of the optical potential with the zero absorption, are very close to the experimental ones. At $E_{lab} = 170$ MeV, the first Airy minimum predicted at $\theta_{c.m.} \approx 80°$, as discussed above, could not be clearly identified in the measured angular distribution. However, this predicted A1 minimum falls on the empirical A1 line shown in Fig. 5, and this result supports the WS1 or folding family of the real optical potential as the most realistic one.

With the position of the first Airy minima well established, one can immediately identify in Fig. 5 the supernumerary Airy minima of the second and third order. In the data at $E_{lab} = 132$ MeV, the prominent minimum observed at $\theta_{c.m.} \approx 82°$ (as extracted from the new data) was suggested earlier [15] as the second Airy minimum. The systematics shown in Fig. 5 confirms now this conclusion. The third order Airy minima in the measured elastic angular distributions at 132 and 170 MeV could also be identified and they agree very well with the A3 line predicted by the OM calculation using the WS1 set of the optical potential (with $W = 0$).

For a complete systematics, it is of interest to discuss the volume intergrals of both the real ($J_V$) and imaginary ($J_W$) parts of the $^{16}O + ^{12}C$ optical potential. It is known that these quantities may be much better determined by the data than the individual potentials themselves [1]. In particular, the volume integral of the real potential $J_V$ has been shown to be the key to classify various WS sets of the optical potential (especially at low energies) into discrete potential families which differ from each other by the order of the Airy oscillatory pattern in the calculated elastic cross section, and by the number of nodes sustained by the wave function of relative motion if antisymmetrization is considered (see, e.g., the results obtained for the $^{12}C + ^{12}C$ and $^{16}O + ^{16}O$ systems in
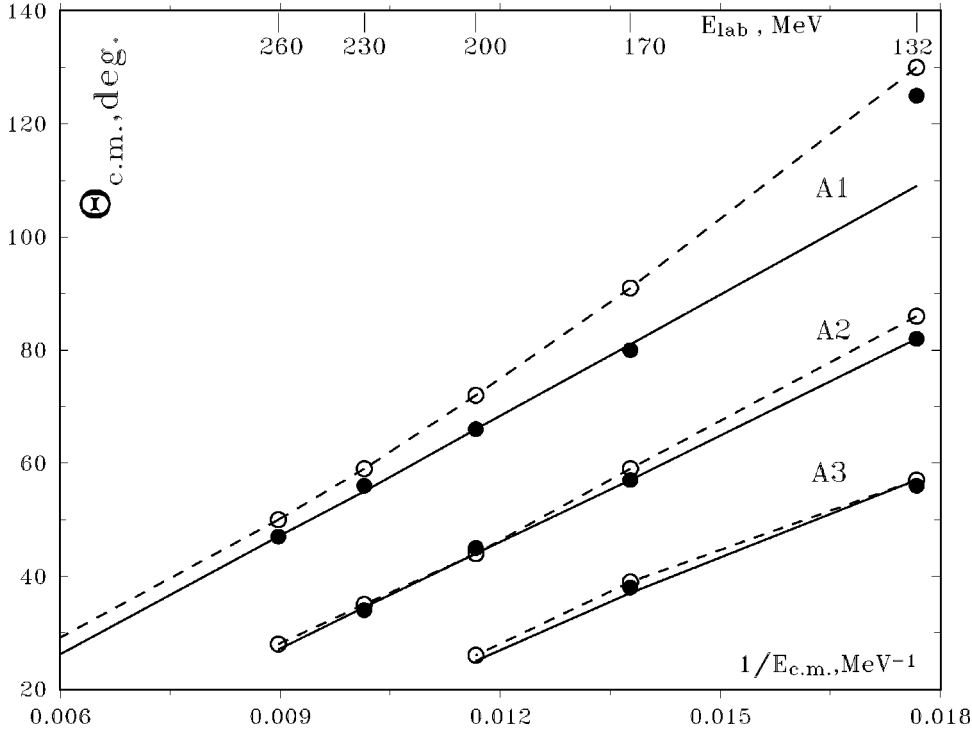
FIG. 5. Positions of the minima (versus $1/E_{c.m.}$) in the measured elastic $^{16}O + ^{12}C$ elastic cross sections, which can be considered as Airy minima (solid circles). The solid straight lines are only to guide the eye. The corresponding minima in the calculated elastic $^{16}O + ^{12}C$ cross sections (open circles connected by dashed lines) which have been obtained using the WS1 set of the optical potential (Table I) with the zero absorption ($W = 0$).

Refs. [7,28]). From the volume integrals $J_V$ and $J_W$ of the best-fit WS1 and the folding potentials given in Table I one finds that they agree with each other within a few percent, and these two potential sets do belong to the same family which generates the Airy structure shown in Figs. 1 and 2.

The WS2 set of the optical potential, which has been shown above to give a wrong order of the Airy oscillation in the elastic cross section, has a volume integral of the real optical potential about 20–30 % larger than that of the WS1 or folding potential. The fact that the volume integral of the imaginary potential is about the same for the WS1, WS2, and folding sets of the optical potential (Table I) clearly shows that the Airy refractive structure is determined entirely by the real potential.

The $J_V$ and $J_W$ values obtained with the WS1 or folding potential also agree closely with the global systematics found for light HI elastic scattering (see, e.g., Fig. 6.7 in Ref. [1]). It is also remarkable that at the incident energy of 200 MeV where the first Airy minimum and the associated primary rainbow are most pronounced in the $^{16}O + ^{12}C$ system, the $J_V$ values obtained with the WS1 or folding potential are around 300 MeV fm$^3$, very close to $J_V$ values obtained for the $^{16}O + ^{16}O$ system at 350 MeV [7,25,28] where the most clear rainbow pattern associated with A1 has been observed for this system.

Finally we note that the best-fit $N_R$ factors for the folding potential are around 0.77 (see Table I) and they reproduce quite well the (realistic) energy dependence of the $J_V$ value. This indicates again the reliability of the folding model to predict the (real) optical potential for a HI system at incident energies from a few MeV/nucleon up to around 100 MeV/nucleon. The more detailed analysis of the energy dependence of $J_V$ and $J_W$ using dispersive relations is now in progress.

## IV. SUMMARY

Differential cross section of the elastic $^{16}O + ^{12}C$ scattering at incident energies of 170, 200, 230, and 260 MeV has been measured over a wide angular range. A well developed nuclear rainbow pattern, more intense than that observed earlier in the (symmetric) $^{12}C + ^{12}C$ and $^{16}O + ^{16}O$ systems, has been established, where up to three strong Airy minima could be identified in each measured elastic angular distribution. The analysis of the new data unambiguously shows that the $^{16}O + ^{12}C$ system is strongly refractive, with the elastic scattering pattern at large angles determined entirely by the far-side scattering. These refractive features are of great importance in studying the energy dependence of the $^{16}O + ^{12}C$ optical potential and testing different theoretical models for this system.

The OM analysis of these experimental data, including remeasured data at 132 MeV was done using both the conventional Woods-Saxon form of the optical potential and the microscopic folding potential (calculated using a realistic effective $NN$ interaction with a density dependence chosen from an extensive study of refractive light HI scattering [5]). At each energy, the best-fit folded potential and the corresponding WS1 potential found in the OM analysis of the data were shown to be of the same potential group of the real optical potential, which is accompanied by a relatively weak absorption. This family of the optical potential for the $^{16}O + ^{12}C$ system was shown to be the most realistic, which consistently generates the evolution of the Airy pattern with the increasing energy.

A strong refractive structure associated with the second Airy minimum (A2) was observed in the elastic $^{16}O + ^{12}C$ data at $E_{lab} = 132$ MeV. The first Airy minimum A1 followed by a broad primary rainbow was found to be most

prominent in the data at $E_{lab} = 200$ MeV, and this (primary) rainbow structure is even stronger than that observed in the famous $^{16}O + ^{16}O$ elastic data at $E_{lab} = 350$ MeV [3,25]. The primary rainbow was predicted by the folding model still to be seen in the elastic $^{16}O + ^{12}C$ scattering at higher incident energies (around 350–500 MeV) and an experimental study of the $^{16}O + ^{12}C$ scattering in this energy region would be of interest. The remnant of A1 and the primary rainbow can also be seen in the analysis of the data at 608 MeV, but it is less unambiguous because at this energy the refractive part of the angular distribution is shifted to such small angles that it becomes mixed with the diffractive part.

The refractive effects studied here for elastic $^{16}O + ^{12}C$ scattering are expected to be present also in the inelastic scattering at the same incident energies. Some preliminary study has been done [29] for the inelastic data at 200 MeV.

A more detailed and consistent theoretical analysis is now in progress.

---

[1] M. E. Brandan and G. R. Satchler, Phys. Rep. **285**, 143 (1997).

[2] M. E. Brandan *et al.*, Comments Nucl. Part. Phys. **22**, 77 (1996).

[3] E. Stiliaris *et al.*, Phys. Lett. B **223**, 291 (1989).

[4] Dao T. Khoa and W. von Oertzen, Phys. Lett. B **342**, 6 (1995); Dao T. Khoa *et al.*, Phys. Rev. Lett. **74**, 34 (1995).

[5] Dao T. Khoa, G. R. Satchler, and W. von Oertzen, Phys. Rev. C **56**, 954 (1997).

[6] Y. Sugiyama *et al.*, Phys. Lett. B **312**, 35 (1993).

[7] Y. Kondō *et al.*, Phys. Lett. B **365**, 17 (1996).

[8] M. E. Brandan and G. R. Satchler, Phys. Lett. B **256**, 311 (1991).

[9] U. C. Voos, W. von Oertzen, and R. Bock, Nucl. Phys. **A135**, 207 (1969).

[10] H. H. Gutbrod *et al.*, Z. Phys. **262**, 377 (1973).

[11] M. E. Brandan and A. Menchaca-Rocha, Phys. Rev. C **23**, 1272 (1981).

[12] M. E. Brandan *et al.*, Phys. Rev. C **34**, 1484 (1986).

[13] P. Roussel *et al.*, Phys. Rev. Lett. **54**, 1779 (1985).

[14] G. R. Satchler, Nucl. Phys. **A574**, 575 (1994).

[15] A. A. Ogloblin *et al.*, Phys. Rev. C **57**, 1797 (1998).

[16] W. von Oertzen and H. G. Bohlen, Phys. Rep., Phys. Lett. **19C**, 1 (1975).

[17] W. von Oertzen (private communication).

[18] Dao T. Khoa, W. von Oertzen, and H. G. Bohlen, Phys. Rev. C **49**, 1652 (1994).

[19] M. E. Farid and G. R. Satchler, Nucl. Phys. **A438**, 525 (1985).

[20] S. A. Goncharov, O. M. Knyazkov, and A. A. Kolozhvari, Yad. Fiz. **59**, 666 (1996) [Phys. At. Nucl. **59**, 634 (1996)].

[21] V. B. Soubbotin and X. Viñas, J. Phys. G **25**, 2087 (1999); M. Ismail, M. M. Osman, and F. Salah, Phys. Rev. C **60**, 037603 (1999); Dao T. Khoa (unpublished).

[22] M. H. Macfarlane and S. C. Pieper, Argonne National Laboratory Report No. ANL-76-11, 1978; M. Rhoades-Brown, M. H. Macfarlane, and S. C. Pieper, Phys. Rev. C **21**, 2417 (1980); **21**, 2436 (1980).

[23] M. E. Farid and G. R. Satchler, Phys. Lett. **146B**, 389 (1984).

[24] R. C. Fuller, Phys. Rev. C **12**, 1561 (1975).

[25] Dao T. Khoa, W. von Oertzen, H. G. Bohlen, and F. Nuoffer, Nucl. Phys. **A672**, 387 (2000).

[26] K. W. McVoy and M. E. Brandan, Nucl. Phys. **A542**, 295 (1992).

[27] J. Knoll and R. Schaeffer, Ann. Phys. (N.Y.) **97**, 307 (1976).

[28] Y. Kondō, M. E. Brandan, and G. R. Satchler, Nucl. Phys. **A637**, 175 (1998).

[29] A. S. Dem'yanova *et al.*, ''Clustering Phenomena in Nuclear Physics,'' in Abstracts of the Reports at the International Conference on Nuclear Physics, St. Petersburg, Russia, 2000 (to be published).